Ferrocene modified g-C_3N_4 as a heterogeneous catalyst for photo-assisted activation of persulfate for the degradation of tetracycline

Zixuan Wang [a, b, 1], Han Wang [a, b, 1], Ziwei Wang [a, b, 1], Danlian Huang [a, b], Hong Qin [a, b], Yangzhuo He [a, b], Ming Chen [c, *], Guangming Zeng [a, b, *], Piao Xu [a, b, *]

[a] College of Environmental Science and Engineering, Hunan University, Changsha 410082, P.R. China.

[b] Key Laboratory of Environmental Biology and Pollution Control, Ministry of Education, Hunan University, Changsha 410082, P.R. China.

[c] Key Laboratory of Reservoir Aquatic Environment, Chongqing Institute of Green and Intelligent Technology, Chinese Academy of Sciences, Chongqing 400714, China.

[*] Corresponding Authors at: College of Environmental Science and Engineering, Hunan University, Changsha 410082, PR China; E-mail addresses: mchensn@hnu.edu.cn (M. Chen), zgming@hnu.edu.cn (G. Zeng) and piaoxu@hnu.edu.cn (P. Xu).

[1] These authors contribute equally to this article.

Abstract

In this study, the oxidative degradation of tetracycline (TC) by ferrocene-modified graphite phase carbon nitride (Fe/g-C_3N_4) activated persulfate (PS) under light-assisted conditions is examined. The materials are characterized by a series of methods such as SEM, TEM, XRD, FTIR, XPS, etc. This article explores the influence of the amount of sulfate, the initial concentration of pollutants, the amount of catalyst, and the pH value on the reaction system. When the amount of PS added reaches 2.5 mM and the catalyst dosage is 1 g L^{-1}, the Fe/g-C_3N_4/PS/Vis exhibit the best performance for tetracycline removal. In 60 min, the removal of tetracycline reaches 93% under its natural pH. In the reaction system acidic neutral conditions are more conducive to degrade TC. The results show that the doping of ferrocene inhibits the recombination of electron-hole pairs in the g-C_3N_4, expands the light response range to speed up the removal rate of tetracycline. At the same time, iron cycle generated by ferrocene modification helps to activate persulfate to produce sulfate radicals with strong oxidizing properties. Sulfate radicals, hydroxyl radicals, superoxide radicals and holes are the main active species proved by ESR test and the quenching experiments. The synergy between photocatalysis and PS activation promotes the production of active species and the tetracycline removal. The results show that the Fe/g-C_3N_4 composite material activated persulfate under visible light is an effective method to remove tetracycline from water.

Keywords：Tetracycline degradation; Persulfate; Photocatalytic activation; Ferrocene modification.

1. Introduction

In recent years, urbanization process is speeding up, along with the rapid economic development, but also accompanied by a series of environmental problems [1]. Antibiotic is an important drug to kill or inactivate pathogenic bacteria in animal and humans [2]. Furthermore, antibiotic has been widely used in aquaculture and livestock and poultry industries as growth promoters and veterinary drugs [3]. Statistics show that the European Union consumes about 5000 tons of antibiotics each year, of which tetracycline antibiotics are as high as 2300 tons; in the United States, tetracycline antibiotics account for 15.8% of the entire antibiotic market share; China is a large country in the production, sales and use of antibiotics, with annual export volume up to 1.34×10^7 kg [4-5]. Nowadays, antibiotic pollution of wastewater has become a current prominent environmental risk problem, which has attracted the attention of some researchers [6-9]. Tetracycline (TC) as one of the most common antibiotics has been widely used in animal husbandry, agriculture and medicine [10]. Compared with other antibiotics, TC has strong persistence in the environment and is difficult to degrade, so its residual time in the environment is long and is more likely to affect human health [11]. However, it is difficult to completely remove the antibiotics in the wastewater with conventional water treatment technology.

Nowadays, advanced oxidation processes (AOPs) has received extensive attention in the removal of organic pollutants due to its low cost, environmental friendliness and simple reaction conditions [12]. Advanced oxidation processes (AOPs) based on sulfate radicals are receiving more and more attention due to their high purification efficiency [13]. Many methods are used to activate PMS to remove pollutants, including transition metal doping, metal oxide modification, and photocatalysis [14]. Photocatalysis is the optical-driven chemical process on the surface of the catalyst, which can convert solar energy into chemical energy, generate holes and electrons, degrade various organic pollutants to remediate the environment [15]. However, photocatalysis technology suffers from insufficient absorption of solar light, high recombination rate of electron-holes pairs and weak mineralization efficiency [16]. Persulfate activation which generate sulfate radicals ($SO_4^{\bullet -}$) possessing stronger oxidation capacity compared with •OH radicals [17]. Activate peroxymonosulfate (PMS) or peroxodisulfate ($S_2O_8^{2-}$) by ultraviolet light, alkali or transition metal to generate sulfate radicals [18]. However, its practical application is still limited by intensive energy input, secondary pollution and low cycle ability [19]. Therefore, many studies combined photocatalysis and persulfate oxidation technologies to synergistically degrade antibiotics [20-21]. Undoubtedly, the key issue for great persulfate activation under visible light irradiation is the reasonable design of catalysts [22].

Some classic semiconductor photocatalysts, such as TiO_2, ZnO, and SnO_2, have become research hotspots due to their stable chemical properties, photocorrosion resistance, and environment friendly [23]. However, the electron-hole recombination rate is high, wide band-gap and low solar energy utilization limit the application [24]. Metal-free semiconductor graphitic carbon nitride (g-C_3N_4) with good chemical stability and thermal stability has been widely used in photocatalytic degradation of organic pollution [25]. g-C_3N_4 is also a newly emerging photocatalyst for advanced oxidation of sulfate radicals [26]. The photogenerated electrons in g-C_3N_4 are excited to break the peroxy (O-O) bond in the persulfate and the oxidant, and generate active free radicals, that is, sulfate free radicals and hydroxyl free radicals except superoxide free radicals [27]. The g-C_3N_4-mediated persulfate photocatalytic activation synergistic mechanism can ensure the generation of hydroxyl radicals, overcome the low reduction potential of g-C_3N_4, and increase the degradation reaction rate [28]. However, g-C_3N_4 with rapid electron and hole recombination, small specific surface area, low quantum yield and other shortcomings usually shows limited the application of photocatalysis-persulfate activation [29]. In this regard, many researchers have devoted to modifying graphite-phase carbon nitride through metal doping, semiconductor connection, heterostructure fabrication, or modified carbon material to improve its photocatalytic performance [30]. Activation of persulfate with transition metals such as copper, iron, and nickel has proven to be an effective way to produce sulfate [31]. Jyun-Ting Lin et al. (2017) have investigated that chemical modification of g-C_3N_4 by iron doping is an effective way to solve this problem [32]. Huang et al. (2019) modified g-C_3N_4 through Fe_3O_4 to construct a heterojunction, which improved its ability to activate persulfate to degrade pollutants [33]. From an environmental protection perspective, iron is a relatively green metal, which is conducive to sustainable environmental restoration [34]. The discovery of ferrocene has brought metal organic chemistry into a new field [35]. Each ring of ferrocene is aromatic and prone to electrophilic substitution reactions. And it has good stability and low toxicity, and has a variety of physiological activities [27]. At the same time, ferrocene has excellent reversible oxidation-reduction performance and electrochemical activity [36]. In addition, the study on the removal of tetracycline by using ferrocene as the iron source to synthesize iron-modified graphite phase carbon nitride has not been reported.

In this study, TC was used as the target pollutant to study the effect of ferrocene modified carbon nitride on antibiotics removal and the mechanism. Composite materials were synthesized by thermal polymerization and characterized by various methods. This paper focuses on the role of Fe and carbon nitride in the optimized Fe/g-C_3N_4 skeleton and the possible mechanism of tetracycline removal. The degradation efficiency based on different PS concentration, initial TC concentration, catalyst dosage and solution pH were all studied. And the catalytic activity, stability and repeatability of the catalyst were investigated at the same time.

2. Material and methods

2.1. Chemical materials

The reagents used in this study were all analytical grade without further purification. Melamine and ethyl alcohol were obtained from Sinopharm Chemical Reagent Co., Ltd. (Shanghai, China), ferrocene were obtained from Spectrochem, sodium peroxodisulfate (PS; ≥98%), Tetracycline (TC) were obtained from Aladdin Biochemical co., Ltd. (Shanghai, China). The deionized water (DI water, resistivity of 18.2 MΩ cm^{-1}) was used as solvent in the all experiments.

2.2. Preparation of materials

2.2.1. Synthesis of graphitic carbon nitride (g-C_3N_4)

g-C_3N_4 was synthesized by a traditional polymerization method [37]. Briefly, 2 g of melamine was put in a ceramic covered crucible; calcined in a muffle furnace at 550 °C with a heating rate of 2.3 °C min^{-1}, and maintained for 4 h in air; cooled down to room temperature; collect and grind to obtain g-C_3N_4 powder.

2.2.2. Preparation of the composite

Composite of Fe/g-C_3N_4 was synthesized by mixing melamine and ferrocene (Fig. 1). For a typical process, a known amount of ferrocene was mixed with 2 g of melamine in a crucible at 550 ℃ for 4 h with a heating rate of 2.3 ℃ min^{-1}, Different percentages of ferrocene in the Fe/g-C_3N_4 composites were tuned to be 1.0%, 2.5%, 5.0%, 7.5%, 10.0% and 15.0% by adding suitable amount of ferrocene. After cooling to 25 ℃, they were dried and grinded to obtain Fe/g-C_3N_4 powder.

2.3. Characterization

The samples morphologies were recorded with a scanning electron microscopy (SEM, Hitachi S-4800, Japan). The surface morphology of the samples was measured by transmission electron microscope (TEM). The crystal structures of ferrocene/g-C_3N_4 were determined by X-ray power diffractometer (XRD, Shimadzu XRD-6000, Japan), equipped with Cu Ka radiation in the region of 2θ from 5° to 80°. The infrared spectra were recorded by a fourier transform infrared spectrophotometer (FT-IR). The elemental mappings of the samples were identified by X-ray photoelectron spectroscopy (XPS) on an Escalab 250Xi spectrometer with an Al-Kα X-ray source. The UV−vis diffuse reflectance spectroscopy (UV-DRS) was carried out on a Cary 300 UV−vis spectrophotometer in the wavelength range from 300 to 800 nm. The electron spin resonance (EPR) signals of the free radicals were recorded by a JEOL JES-FA200 Spectrometer.

2.4. Experimental procedures

Under visible light irradiation, TC was degraded by synthetic materials and its photocatalytic oxidation activity was studied. The visible light source was provided by a PLS-SXE 300 W Xenon lamp, and its light density parameter was 0.33 W cm^{-2}. In detail, 0.05 g of the catalyst was dispersed in the 50mL pollutant reaction solution and irradiated it with light. In order to establish the adsorption-desorption equilibrium, the mixture was stirred for 30 minutes in the dark firstly. Then, a certain concentration of PS was added dropwise to the sample and stirred for 60 minutes under light conditions. In order to study the effect of pH, the reaction solution was adjusted by using 0.1 M NaOH and 0.1 M HCl. Then the reaction suspension was taken out by 5 ml syringe at a given interval time and filtered using a 0.45 μm membrane filter, and then analyzed by a Shimadzu UV-2700 spectrophotometer to record the concentration of TC (357 nm). By changing the reaction conditions, such as the catalytic dose, initial TC concentration, proportion of iron doping in the composite material and the pH on the reaction system were studied. Collect the finished catalyst and clean it several times with deionized water and anhydrous ethanol to remove surface contaminants and impurities for next use. Four consecutive cycles of TC removal were performed.

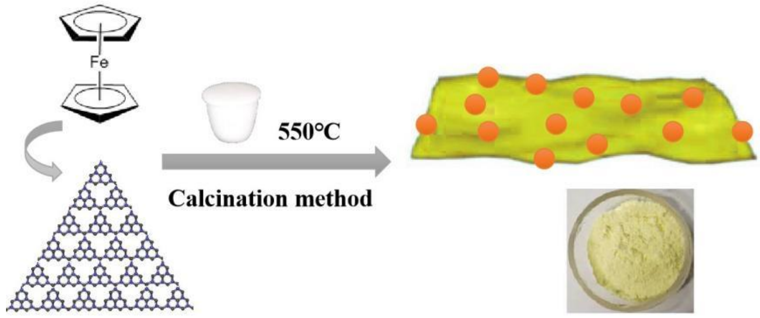

Fig. 1. Construction of Fe / g-C_3N_4 heterojunction

3. Results and discussion

3.1. Characterization of the catalysts

The morphologies and microstructures of the as-prepared materials were characterized by SEM and TEM. Fig. 2 presented that the prepared g-C_3N_4 were mainly stacked by lamellar structures with micron dimensions. During the calcination process, some ferrocene adheres to the surface of graphite phase carbon nitride, and some was embedded in its structure. The majority of g-C_3N_4 exhibited irregular and thick features, while the iron-doped g-C_3N_4 had a significantly smaller particle size and was composed of smooth paper folded sheets, similar to the morphology of graphene nanosheets. Previous literature reports showed that iron atoms played a very important role in the condensation of g-C_3N_4 and the formation of nanostructures. Further, from TEM images (Fig. 3), attached nanoparticles could be clearly seen on the surface of the g-C_3N_4 sheet and inside its structure, which were converted from the ferrocene during the calcination process. Meanwhile, the TEM-EDS mapping results in Fig. 4 showed that carbon, nitrogen, oxygen and iron were almost uniformly distributed on the surface of the catalyst, which proved that Fe was successfully introduced into Fe/g-C_3N_4 composite material once again. The above results indicated that Fe/g-C_3N_4 composite had been synthesized by calcination. Moreover, the ferrocene-modified g-C_3N_4 had a high specific surface area (Fig. 5), which provided more adsorption sites and active centers for the photocatalytic reaction. The chance of pollutants coming into contact with the composite catalyst was increased, and the active species produced in the reaction process had more room for action.

Fig. 5 exhibited the N_2 adsorption and desorption curves of g-C_3N_4 and Fe/g-C_3N_4 composites. It could be seen in the figure that the N_2 adsorption and desorption curves of the two samples conform to the typical type II isotherm [38]. When the relative pressure was in the range of 0.4-1.0, the catalyst had a H3 hysteresis loop, which indicated that there were macropores in the g-C_3N_4 and Fe/g-C_3N_4 composites [39]. This might be due to the accumulation of large particles to form random interstitial pores. The specific surface areas of g-C_3N_4 and Fe/g-C_3N_4 composites were 10.4395 m^2 g^{-1} and 18.076 m^2 g^{-1} respectively (Table 1). Compared with the specific surface area of g-C_3N_4 monomer in the literature, the carbon nitride obtained by calcination of melamine at 550 ℃ had a larger specific surface area. It might be because melamine produces CO_2, CO, H_2O and other gases under high conditions, resulting in a loose structure on the surface of the material [40]. The ferrocene modified g-C_3N_4 composite material had an increased specific surface area, which provided a larger space for the catalytic reaction, and further explains the reason for the high-quality photocatalytic effect of the composite material.

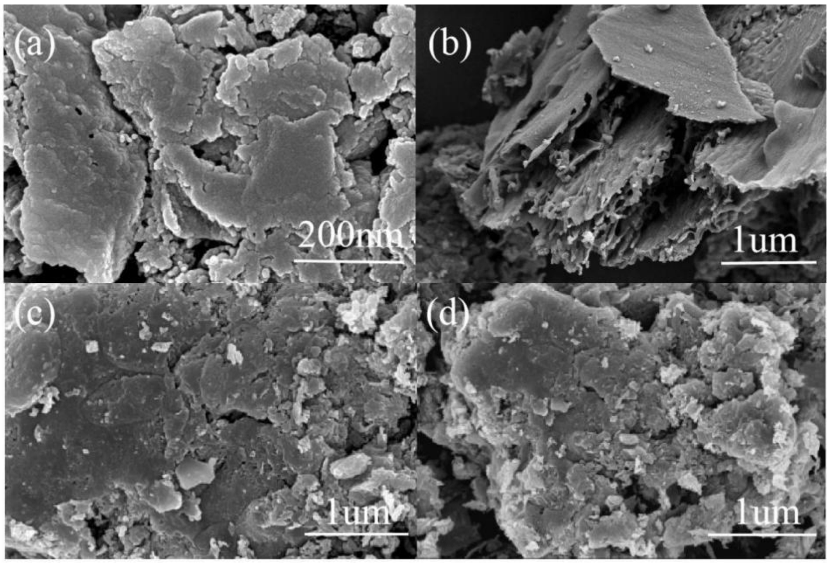

Fig.2. SEM images of g-C_3N_4 (a-b) and Fe/g-C_3N_4 (10%) (c-d) samples.

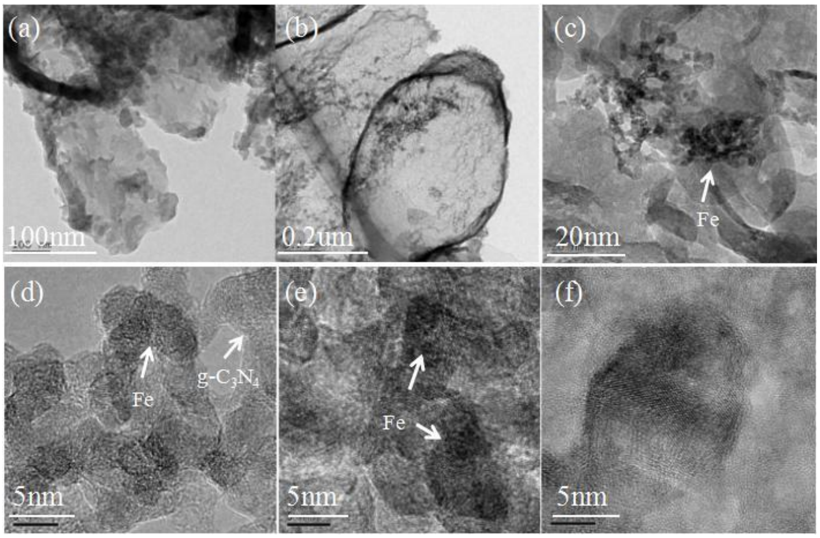

Fig. 3. TEM micrograph images of g-C_3N_4 (a), Fe/g-C_3N_4 (10%) (b-c), and crystal structure of the Fe/g-C_3N_4 (10%) (d-f).

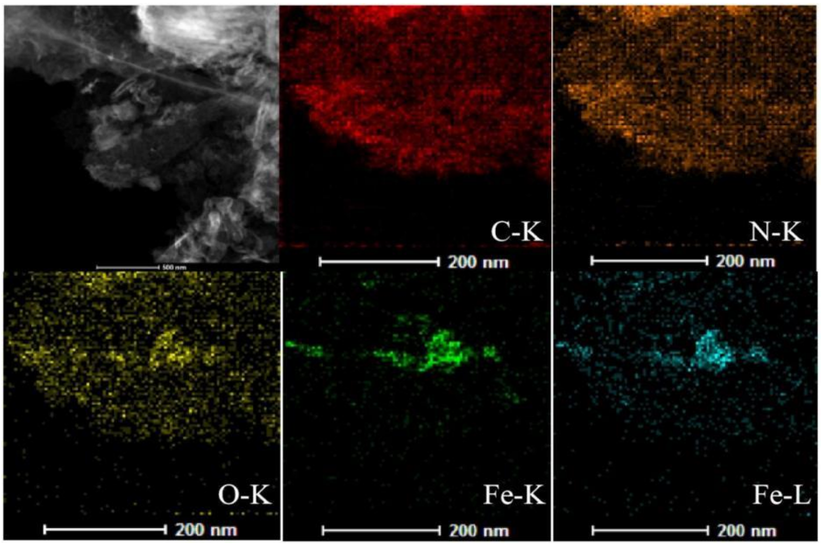

Fig. 4. TEM-EDS elemental mapping images of Fe/g-C_3N_4 (10%).

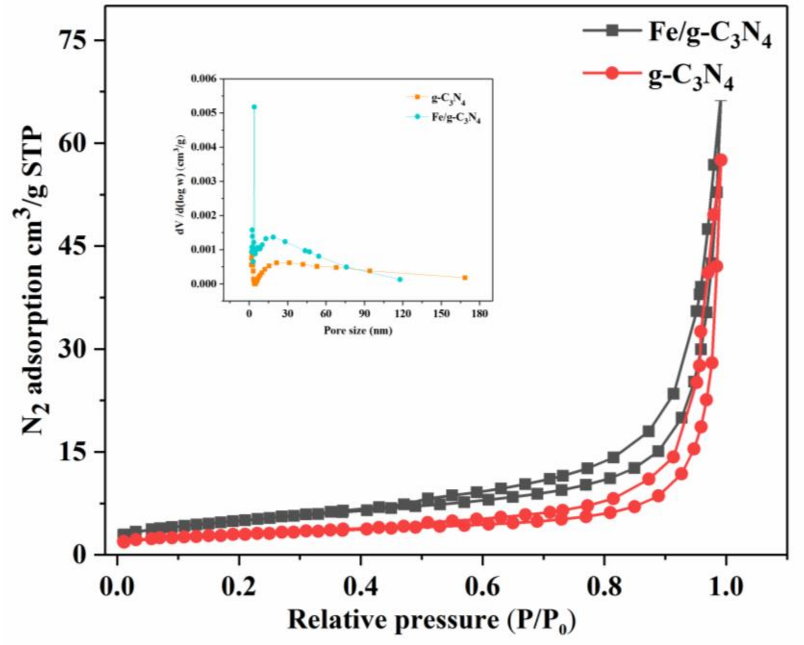

Fig. 5. N_2 adsorption-desorption isotherm of g-C_3N_4 and Fe/g-C_3N_4 (10%) samples.

Table 1

Physicochemical properties of the synthesized pristine g-C_3N_4 and Fe/g-C_3N_4 (10%).

Activators	BET specific surface area ($m^2\ g^{-1}$)	Pore volume ($m^3\ g^{-1}$)	Average pore radius (nm)
g-C_3N_4	10.4395	0.088987	21.5
Fe/g-C_3N_4 (10%)	18.0076	0.103616	21.6

The XRD patterns (Fig. 6a) presented the crystal structure information of g-C_3N_4

and Fe/g-C_3N_4 composites. Same as the previous research reports, all samples had an enhanced diffraction peak at 27.4 °and 13.1 ° [41]. The characteristic peaks at 13.1 ° and 27.4 ° corresponded to the (100) crystal plane and (002) diffraction surface of g-C_3N_4, which was caused by the periodic arrangement of crystal planes in the layers and the stacking of conjugated aromatic rings between the layers [42]. There were three obvious diffraction peaks at 2θ = 18.1 °, 41.3 ° and 57.0 °, corresponding to the (111), (400) and (511) diffraction planes respectively, which were similar to the structure of Fe_3O_4 reported in the previous literature [43]. It showed that ferrocene transforms into iron oxide during the calcination process, mainly in the form of Fe_3O_4 [44]. The XRD pattern of Fe/g-C_3N_4 was similar to the original g-C_3N_4. With the increase of iron doping, the (001) peak of g-C_3N_4 increases, indicating that iron causes slight changed in the graphite layer of g-C_3N_4 structure, resulting in enhanced crystallinity of g-C_3N_4 [45]. In the composite catalyst, the peak position of the characteristic peak of g-C_3N_4 did not change significantly, indicating that the ferrocene modification did not significantly change the crystal structure of g-C_3N_4, which was beneficial to the photocatalysis of the composite catalyst. We could see that there are no other impurity peaks in all samples, which proved that the composite catalyst was composed of an iron-containing compound phase and a g-C_3N_4 phase. The sample had high purity and had been successfully prepared.

The FTIR diagram of Fe/g-C_3N_4 composites was shown in Fig. 6 b. For g-C_3N_4, a series of diffraction peaks occur at 1200-1600 cm^{-1}, which was a very classical stretching pattern for CN heterocyclic compounds [46]. The strong vibration peak at

810 cm^{-1} was caused by the bending vibration of the Heptazine ring, indicating that the synthesized g-C_3N_4 was mainly composed of triazine ring structure [47]. The diffraction peak of Fe/g-C_3N_4 composite was slightly shifted. The extensive absorption peak band in 3200 cm^{-1} was derived from the stretching vibration of N-H bond in g-C_3N_4, indicating the presence of incomplete polymerization of amino in the synthesized g-C_3N_4 [48]. The diffraction peak of Fe/g-C_3N_4 (10%) composite was shifted to 3162 cm^{-1}, indicating that ferrocene and g-C_3N_4 interact during calcination. The FTIR diagram of Fe/g-C_3N_4 composite material did not deviate significantly, surface iron doping did not change the structure of carbon nitride, and there was no obvious iron compound diffraction peak, which was also due to the low doping amount of Fe in the composite material.

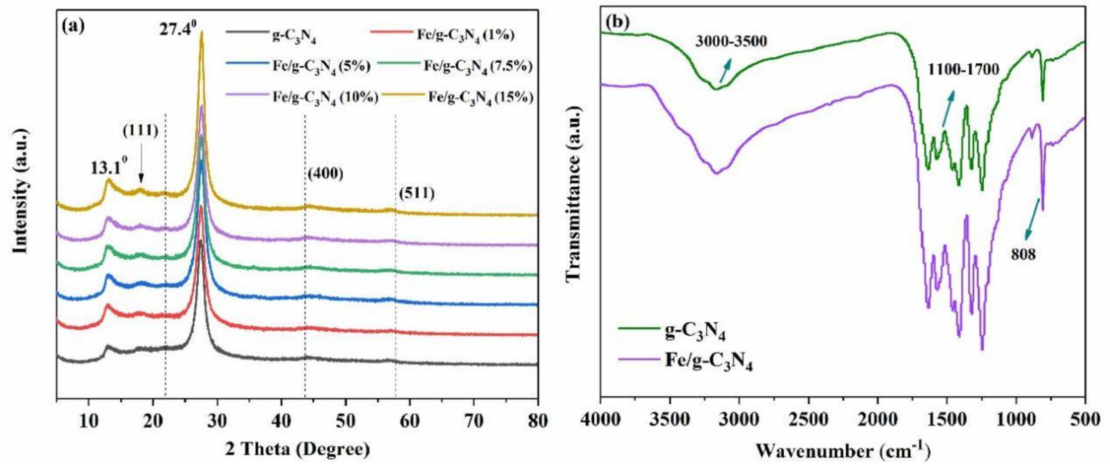

Fig. 6. (a) XRD patterns of g-C_3N_4, Fe/g-C_3N_4 (1%), Fe/g-C_3N_4 (5%), Fe/g-C_3N_4 (7.5%), Fe/g-C_3N_4 (10%), and Fe/g-C_3N_4 (15%), and (b) The FTIR spectra of g-C_3N_4 and Fe/g-C_3N_4 (10%)。

In order to explore the element composition, internal structure and chemical bonds of the synthetic material, the material was analyzed by XPS spectrum. Fig. 7a showed the full spectrum of g-C_3N_4 and Fe/g-C_3N_4, in which the obvious peaks of C, N, O, and Fe could be detected. C and N elements are mainly derived from g-C_3N_4, and the presence of Fe is caused by ferrocene doping. Although g-C_3N_4 and ferrocene did not contain oxygen, the detection of oxygen in graphite phase carbon nitride had been reported by many studies [49]. It was attributed to physical oxygen absorption, and the material was also doped in calcination at high temperature. The C1s core-level spectrum was shown in Fig. 7b, and two characteristic peaks appear at 288 and 284.9eV, which correspond to C=N and C=C respectively [50]. Three characteristic peaks of N element in different chemical forms at 398.4, 399.1 and 400.5 eV (Fig. 7c), which were attributed to the SP^2 hybridization of the connected C atoms in the C=N-C structure, the connected N atoms in the N-$(C)_3$ structure, and the N atoms in the partially polymerized C-N-H structure respectively, and the action of the N-H side group [51]. The C1s and N1s spectra of Fe/g-C_3N_4 also had similar laws. Compared with g-C_3N_4, the binding energy of Fe/g-C_3N_4 obviously shifted to the lower energy level [52]. This was because the chemical environment of carbon nitride has changed after ferrocene doping. The electrons in the lone electron pair of the nitrogen atom in g-C_3N_4 were transferred to the iron atom, which causes the electron density of the nitrogen atom to decrease, which caused the electrons in C-N to move toward the N atom, resulting in the decrease of the C atom density [53]. The composite state analysis of the Fe element doped on the surface of the composite material, as shown in Fig. 7d, shown two obvious diffraction peaks at 723.8 and 710.7 eV, corresponding to the hybridization of Fe elements $2P^{1/2}$ and $2P^{3/2}$, respectively [54]. This indicates that iron was successfully doped into carbon nitride, which further verified the existence of iron and retained the divalent state of iron in ferrocene.

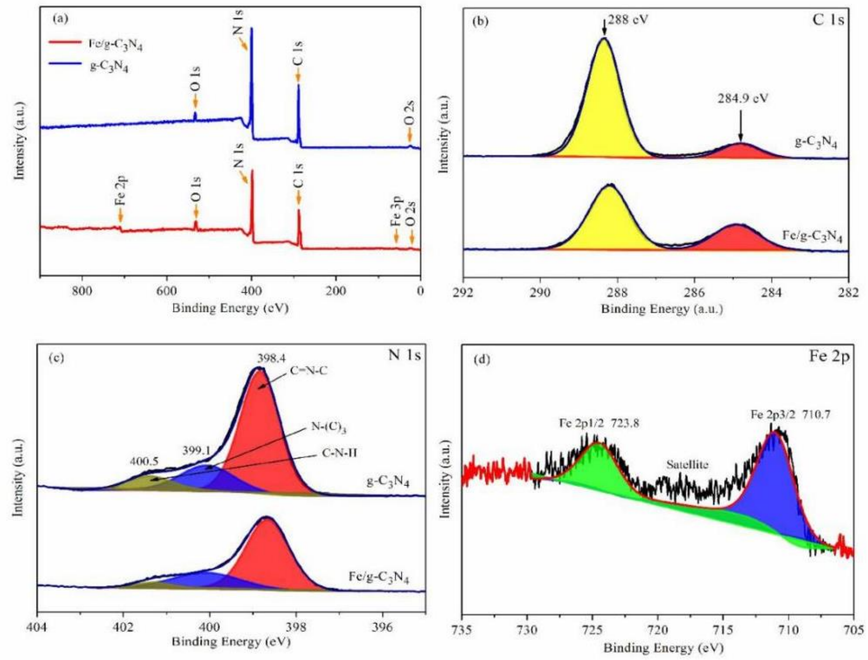

Fig. 7. XPS analyses of g-C_3N_4 and Fe/g-C_3N_4 (10%) samples: (a) full-survey, (b) C1s core-level, (c) N1s core-level and (d) Fe2p core-level spectrum.

3.2. Optical property

The optical properties of the previously prepared g-C_3N_4 and Fe/g-C_3N_4 materials were studied by UV-vis diffuse adsorption spectrum. As shown in Fig. 8a, electrons transition from the valence band formed by the N2p orbital of g-C_3N_4 to the conduction band formed by the C2p orbital [55]. g-C_3N_4 exhibits a typical semiconductor light absorption capacity, and its absorption band edge was located at about 450 nm, showing a capability of utilizing solar spectrum energy with a wavelength less than 450 nm [35]. After ferrocene modification, the absorption band of Fe/g-C_3N_4 was around 550 nm, with a significant red shift. This was the doping of iron ions into the g-C_3N_4 lattice, which affects the electronic structure of graphite phase carbon nitride and changes its optical properties. It could be clearly seen in the figure that the ferrocene doped composite material could greatly broaden the light absorption range of g-C_3N_4, which was beneficial to its use of sunlight and improves the photocatalytic performance.

The combination of photogenerated carriers greatly affects the performance of photocatalytic activation system. Fig. 8b illustrated the photoluminescence (PL) spectra of different photocatalysts. The figure shown the PL spectra of g-C_3N_4 and Fe/g-C_3N_4 composites with different proportions at about 450 nm when excited at 320 nm [56]. It could be seen that the PL peak of the original g-C_3N_4 material was the strongest, indicating that the photogenerated electron and hole pair recombination rate is high. With the doping of Fe, the PL peak of Fe/g-C_3N_4 composite material gradually weakens, which was because the introduction of iron could effectively inhibit the photocarrier recombination and accelerate the electron migration, so as to promote the photocatalysis and facilitate the effective removal of TC. Among them, the PL peak value of Fe/g-C_3N_4 (10%) composite material was the weakest, indicating that Fe/g-C_3N_4 (10%) photogenic carrier composite rate was the lowest, which further proves that Fe/g-C_3N_4 (10%) composite material was the best composite ratio for effectively removing TC in water.

The band gap (Eg) of g-C_3N_4 and Fe/g-C_3N_4 (10%) were 2.59 eV and 2.18 eV, respectively, by analyzing the UV-visible diffuse reflectance spectra (Fig. 9a). Fe/g-C_3N_4 (10%) photocatalyst had a narrower band gap than g-C_3N_4, and could generate more photogenerated electrons under visible light irradiation. Using the Mott Schottky spectrum (Fig. 9b), the conduction band values of g-C_3N_4 and Fe/g-C_3N_4 (10%) had CB potentials of -0.80 eV and -0.43 eV, respectively. According to the formula E_{CB} = E_{VB}-Eg, the valence band (VB) values of g-C_3N_4 and Fe/g-C_3N_4 (10%) were 1.79 eV and 1.75 eV, respectively [57]. Where E_{VB}, E_g, E_{CB} were the band gap energy, VB potential and the band gap potential CB potential, respectively. The detailed positions of the VB and CB bands of Fe/g-C_3N_4 (10%) were shown in Fig. 9c.

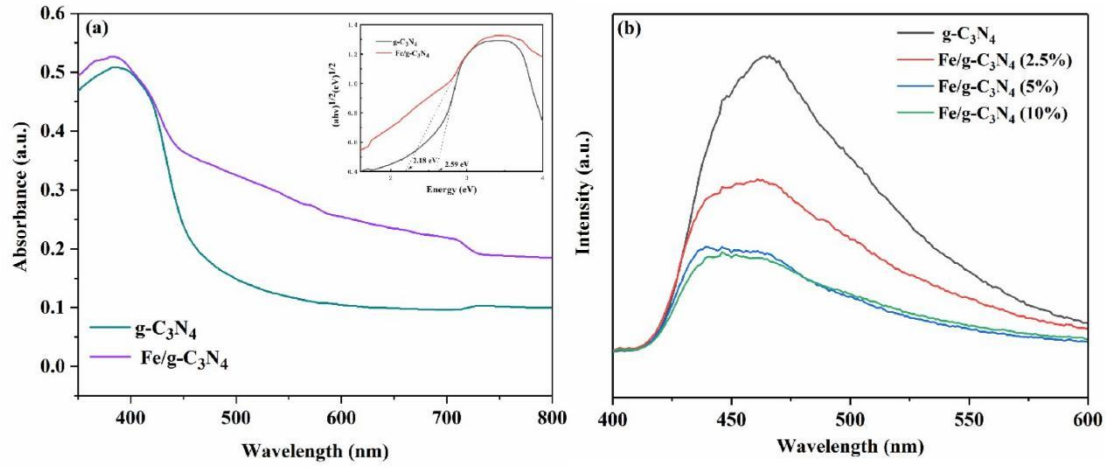

Fig. 8. (a) UV–vis diffuse reflectance spectra of the as-prepared g-C_3N_4 and Fe/g-C_3N_4 (10%) samples and (b) Photoluminescence spectra of the as-prepared samples.

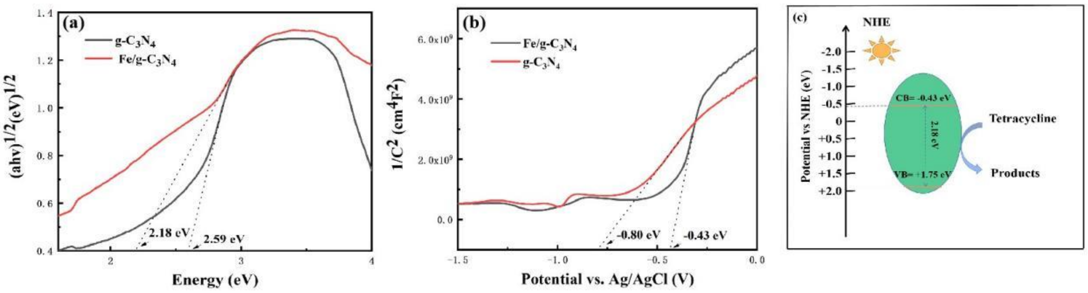

Fig. 9. band gap of g-C_3N_4 and Fe/g-C_3N_4 (10%), (b)Mott Schottky spectrum of g-C_3N_4 and Fe/g-C_3N_4 (10%), (c) Possible mechanism of Fe/g-C_3N_4 (10%) for TC degradation.

3.3. Catalytic performance

3.3.1. TC removal in different systems

As a typical antibiotic, TC has been widely used in agriculture, animal husbandry, and pharmaceutical industries [58]. From Fig. 10a, PS could not directly degrade TC, nor could it be stimulated directly under visible light. From this we concluded that PS alone had little effect on the removal of TC, indicating that PS was difficult to oxidize TC and the photolysis effect of TC was weak under visible light conditions for its high stability. The removal rate of TC was negligible in the PS/Vis system without catalyst. In the Fe/g-C_3N_4/PS system, the removal rate of TC within 60 min was higher than that without catalyst, indicating that the presence of catalyst could promote the removal of TC, it was also possible that the presence of the catalyst could activate PS to remove TC. When Fe/g-C_3N_4 (10%) reacted alone in the catalytic system, the removal rate of TC was relatively low. The degradation rate of TC in Fe/g-C_3N_4/PS system and Fe/g-C_3N_4/Vis system was improved compared with the system with only catalyst, because the catalyst could activate PS to produce hydroxyl radicals and sulfate radicals, *etc*. Light could promote the degradation of pollutants, but its enhancement effect was not great. In the Fe/g-C_3N_4/PS/Vis system, the TC could be removed quickly, and after 30 min of visible light irradiation the removal of TC reached 80%, indicating that light could promote the activation of PS. In the Fe/g-C_3N_4/PS/Vis system, the pollutant could be almost completely degraded. When Fe/g-C_3N_4 activated PS, light accelerated the activation of PS.

3.3.2. Effect of different amounts of iron doping

As depicted in Fig. 10b, the degradation effect became better when the iron doping increased, and Fe/g-C_3N_4 (10%) had the best degradation effect. Previous studies have demonstrated that metal doping could adjust the morphology and crystal phase of g-C_3N_4, create oxygen vacancies or construct heterogeneous structures to enhance the photocatalytic activity of the catalyst [59]. Pure g-C_3N_4 were restricted by its high recombination rate of light induced e^{-}/h^{+}, while carbon nitride modified by ferrocene could effectively separate photogenic electrons from holes, improve photoquantum yield, and greatly enhance its removal effect [60]. When the iron proportion was increased again, the TC removal decreases. This was because Fe ions adsorbed on the surface of the catalyst compete for photo-generated electrons. Excess Fe ions would capture more e^{-} and carry out iron ion valence conversion, which affected the activation of PS by the catalyst, thereby reducing the number of active free radicals and effecting the removal of TC.

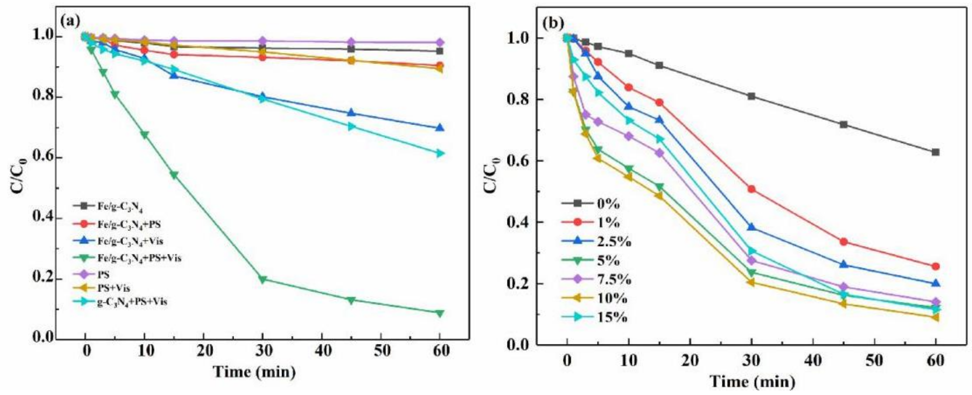

Fig.10. (a)Degradation performance of catalysts in different systems. (b)Degradation performance of catalysts with different amounts of iron doping. Experimental conditions: $[Fe/g\text{-}C_3N_4]_0 = 1.0$ g L^{-1}, $[TC]_0 = 40$ mg L^{-1}, $[PS]_0 = 2.5$ mM, and T = 25 ℃.

3.3.3. Effect of PS concentration

This experiment was conducted to study the removal effect of tetracycline at different PS concentrations (1.0-3.0 mM). When the concentration of PS increased from 1.0 mM to 2.5 mM, the removal rate of TC increased to 93.0%. When PS concentration was higher than 2.5 mM, the removal rate of TC was reduced to 79.0% (Fig. 11a). The results could be explained by the following factors: when the concentration of PS increased, the catalyst could activate more PS and produce more sulfate radical for the oxidation and removal of tetracycline. Many studies had shown that excessive $SO_4^{\bullet-}$ free radicals would undergo self-quenching reactions or react with HSO_5^- to generate $SO_5^{\bullet-}$ free radicals with weaker oxidizing ability, which leads to the $SO_4^{\bullet-}$ involved in the reaction reduced and caused the reactivity was weakened, thereby the TC removal rate decreased [61]. Therefore, 2.5 mM PS was used in the subsequent experiments.

3.3.4. Effect of TC concentration

As revealed in Fig. 11b, show the removal rate curve of TC at concentration of 20, 30, 40, 50 mg L^{-1}. We could see that the removal rate of TC decreases with the increase of the initial concentration of pollutant. When the initial TC concentration was 20 mg L^{-1}, TC could be almost completely removed within 60 min (97.9%). However, the removal rate of pollutants could still high within 60 min when the concentration of TC increased to 50 mg L^{-1}. It was because the same concentration of catalyst and PS will produce the same number of reactive species, while the high concentration of TC solution needs a longer reaction time to achieve the same removal efficiency. When the reaction time was prolonged, 50 mg L^{-1} TC could be completely degraded based on pre-experimental data, which indicates that Fe/g-C_3N_4

could be used as a catalyst to photocatalyze the high efficiency of PS activation and could be used in the treatment of high-concentration antibiotic wastewater.

3.3.5. Effect of catalyst dosage

For investigating the effect of the amount of catalyst in the process of TC removal by persulfate activation, a set of experiments were carried out with an Fe/g-C_3N_4 dose of 0.2-1.0 g L^{-1}. As depicted in Fig. 11c, when the catalyst dose increased, the TC removal improved. This was because the increase of Fe/g-C_3N_4 concentration would have more reactive sites, thereby generating more strong oxidizing free radicals, which would help the degradation of pollutants. However, when the catalyst concentration continued to increase, the catalytic effect was not obvious, or even slightly decreased. It was attributed to the fact that the high concentration of catalyst leads to the turbidity of the reaction solution and reduces the light transmittance, thus reducing the surface area exposed to light and affecting the photocatalytic effect. Therefore, considering the actual application cost of the catalyst, 1 g L^{-1} was adopted for next experiments.

3.3.6. Effect of pH

In this experiment, the effect of pH on the reaction system was studied. NaOH and HCl at certain concentrations were used to adjust the initial pH of the reaction solution. In Fig. 11d, we could see that with the increase of pH, the removal rate of the TC decreased. But, in the range of pH 3-9, the removal rate of TC was still very high. When pH =11, the removal rate of TC decreased significantly. The results showed that under acidic and neutral conditions, the material could activate persulfate to remove organic pollutants under the light. In alkaline environment, the removal rate was not high, because strong oxidizing $SO_4^{\bullet-}$ reacts with OH^- to produce weak oxidizing •OH, thus weakening the degradation activity of catalytic system.

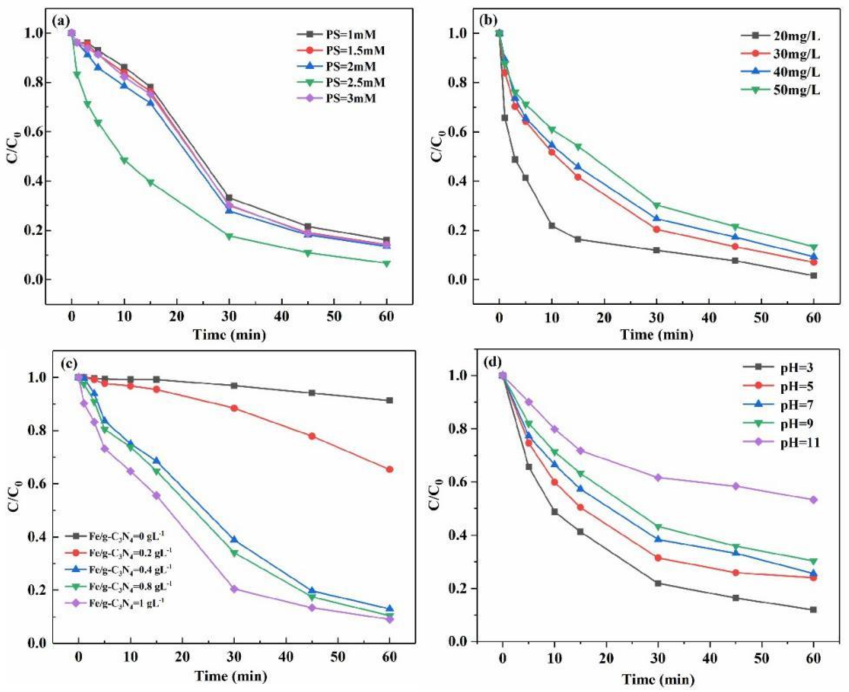

Fig. 11. Effects of (a) PS dosage, (b) initial pollutant concentration, (c) catalysts dosage, and (d) pH on TC degradation by the Fe/g-C_3N_4/PS system. Experimental conditions: (a) $[TC]_0$ = 40mg L^{-1}, [Fe/g-C_3N_4]$_0$ = 1.0 g L^{-1}, and T=25 ℃. (b) [Fe/g-C_3N_4]$_0$ = 1.0 g L^{-1}, $[PS]_0$ = 2.5 mM, and T = 25 ℃. (c) $[PS]_0$ = 2.5 mM, $[TC]_0$ = 40 mg L^{-1}, and T = 25 ℃. (d) [Fe/g-C_3N_4]$_0$ = 1.0 g L^{-1}, $[TC]_0$ = 40 mg L^{-1}, $[PS]_0$ = 2.5 mM, and T = 25 ℃.

3.4. Recyclability and stability

The reusability is an important parameter to determine whether photocatalyst can be used in water remediation. In order to evaluate the recyclability of Fe/g-C_3N_4 composite, five consecutive tests of degradation of tetracycline were conducted under the same reaction conditions. As exhibited in Fig. 12b, the bar chart visually shown the removal efficiency of tetracycline in each cycle, and the difference between each cycle could be clearly seen. After three cycles, the removal efficiency of Fe/g-C_3N_4 was 87.50%, not much different from that of the first experiment. After the fifth cycle, the removal efficiency of the composite was still high. It showed that the stability and recyclability of the material was good, recycling could also be used. Compared with the first cycle, the reduction effect of the fifth cycle might be attributed to the loss caused by the inevitable leaching of the catalyst during the recovery and washing process, and the blockage of the active site covering the surface with tetracycline and its degradation intermediates. As displayed in Fig. 12a, the mineralization efficiency of TC reached 41% within the stimulation range of 60 min of visible light.

In order to further observe the stability of Fe/g-C_3N_4 (10%), the composite catalysts which were cycled four times were analyzed by XRD and FTIR. As presented on Fig. 13, the structure of the catalyst after the cycle did not change much compared with that of the initial cycle. The stability of the composite structure was pretty good, which further explained its excellent catalytic effect.

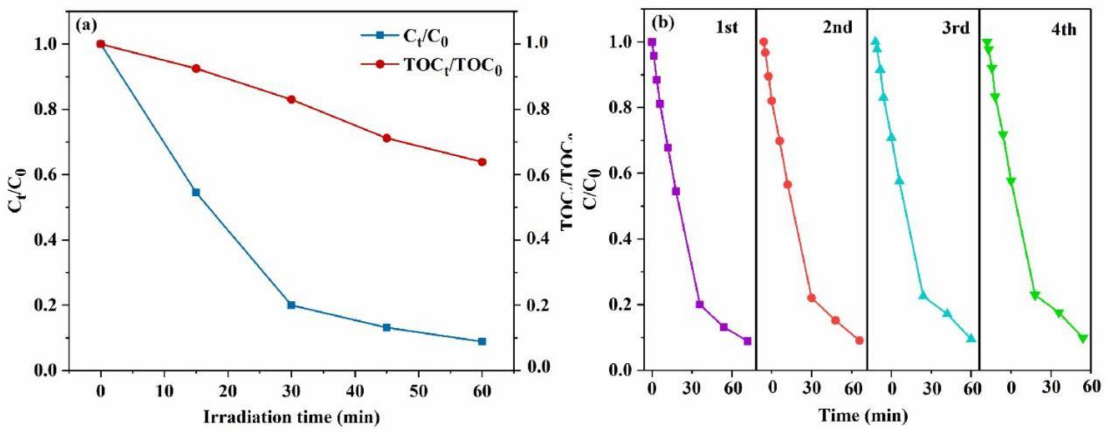

Fig. 12. (a) The photodegradation and TOC removal curves of TC on Fe/g-C_3N_4 (10%) composites. (b) The column chart of degradation efficiency of TC leaching concentration in the photo-assisted PMS activation catalytic processes over Fe/g-C_3N_4 (10%) for five cycles.

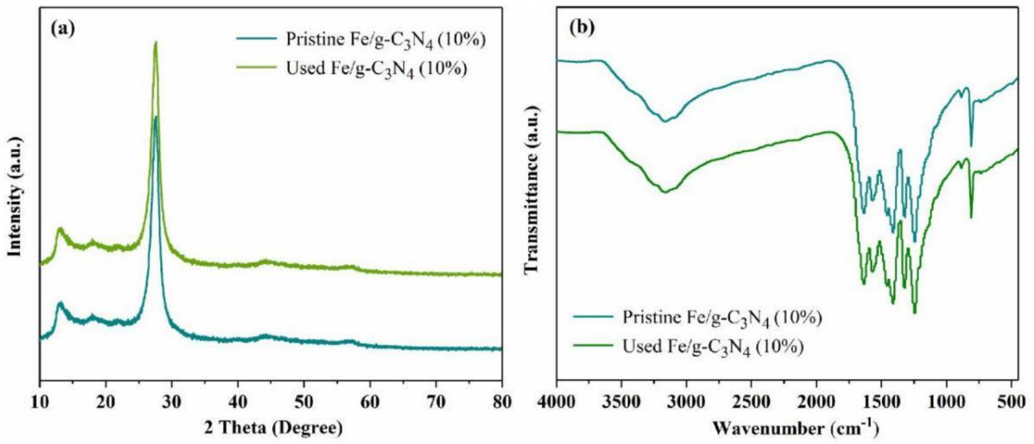

Fig. 13. (a) XRD pattern of Fe/g-C_3N_4 (10%) before and after usage. (b) The FTIR spectra of Fe/g-C_3N_4 (10%) before and after usage.

3.5. TC removal mechanisms by Fe/g-C_3N_4

High temperature, ultraviolet light, and addition of catalyst can activate PS to generate sulfate radicals and hydroxyl radicals, and g-C_3N_4 materials can generate superoxide radicals and holes under visible light irradiation. In order to further study the contribution of active species in the Fe/g-C_3N_4/PS/Vis system, we carried out free radical capture experiments. Tert-butanol (TBA) reacts with hydroxyl radicals faster than sulfate radicals and can selectively quench hydroxyl radicals in the reaction system [62]. Ethanol (EtOH) can react with sulfate radicals ($SO_4^{\bullet-}$) and hydroxyl radicals (•OH) [63]. Therefore, TBA and ethanol were used as trapping agents for hydroxyl radical and sulfate radical. In addition, EDTA-2Na and 1,4-benzene quinone (BQ) were added as hole (h^+) and superoxide radical ($\bullet O_2^-$) quenchers in the control experiment [64]. 1 mol L^{-1} quencher was added to the reaction system. In Fig. 14a, the removal effect of the catalyst dropped to about 30% after adding EDTA-2Na, indicating that the holes had a great influence on the reaction. After adding TBA and EtOH, the removal of TC was obviously inhibited. This was because Fe/g-C_3N_4

activated PMS to produce a large amount of strong oxidizing $SO_4^{\bullet-}$, which promoted the oxidative removal of TC. On the other hand, with the addition of BQ, the removal rate decreased but it was not obvious, indicating that superoxide radicals did not contribute much to the TC oxidation decomposition reaction. In conclusion, in the free radical capture experiment, hydroxyl radicals, sulfate radicals and holes were the main active species in the Fe/g-C_3N_4/PMS/Vis system.

The thermogravimetric curve is shown in Fig. 14b. The ferrocene and g-C_3N_4 interact during the calcination process to form a graphite phase carbon nitride-based composite material doped with iron oxide. The temperature is around 400 ℃, and the end temperature when the mass change reaches the maximum is 550 ℃. It is reported in the literature that melamine begins to decompose at 354 ℃, and ferrocene decomposes at 400 ℃ [65]. Since the two are mixed and calcined, the mixed material starts to decompose at about 400 ℃. The first plateau in the thermogravimetric curve is a mixture of ferrocene and melamine before 400 ℃. Weight loss occurs between 400-550 ℃, and the solid component of the second platform is a mixture of Fe_2O_3, Fe_3O_4 and g-C_3N_4. Combining XPS, TEM-EDS elemental mapping images and XRD characterization, we analyzed that ferrocene was converted to iron oxide during the calcination process, and the main form is Fe_3O_4. And it can be seen from the figure that the composite material maintains the good thermal stability of the ferrocene monomer.

To further prove that hydroxyl radicals, superoxide radicals and sulfate radicals were produced during the reaction, we carried out EPR experiments. The EPR experiment is the most effective method to determine the types of free radicals produced during the removal of tetracycline [66]. As we can see in Fig. 16, under dark conditions, no obvious ESR signals of hydroxyl radicals, superoxide radicals and sulfate radicals were observed, which proved the importance of light to the production of active species in the reaction system [67]. Meanwhile, the characteristic peaks of hydroxyl radicals, sulfate radicals and superoxide radicals fluctuate significantly after light was provided, indicating that these active free radicals could be generated under the excitation of visible light.

In order to study the effect of ferrocene modification on the separation efficiency of photogenerated carriers in g-C_3N_4, a photocurrent experiment was carried out to study the photocurrent response properties of Fe/g-C_3N_4 and g-C_3N_4. The photocurrent test results (Fig. 15) showed that both Fe/g-C_3N_4 and g-C_3N_4 catalysts had photoresponse properties under visible light, but their intensities were different. From the figure, we could see that the photocurrent response intensity of ferrocene-modified g-C_3N_4 was more than twice that of g-C_3N_4 alone, indicating that the iron introduction can help the separation of photogenerated electrons and holes in g-C_3N_4 materials[68] . The efficiency allowed more holes and electrons to participate in the reaction, which was conducive to the conversion between divalent iron and trivalent iron, accelerated the activation efficiency of PS, enhanced the photocatalytic activity, and promoted the removal of tetracycline.

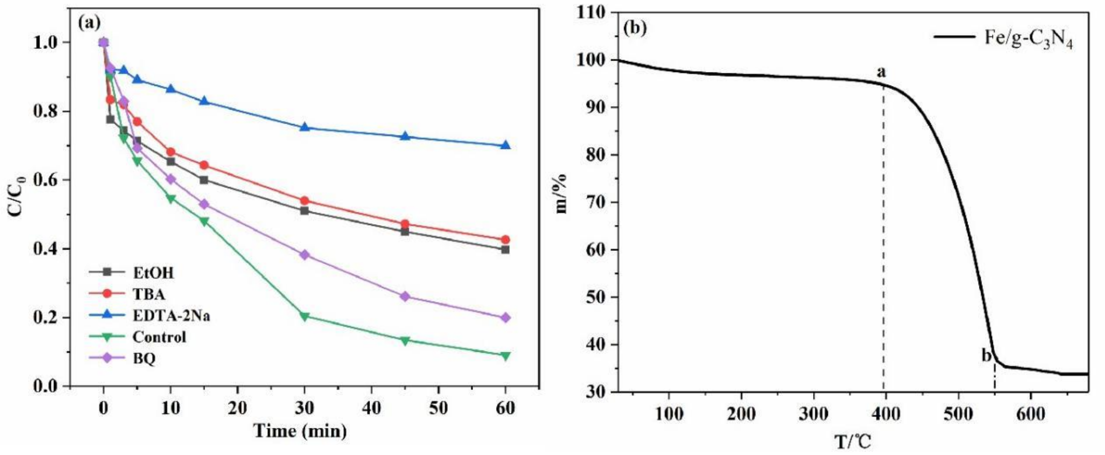

Fig. 14. (a) Effect of EtOH, TBA, EDTA-2Na and BQ as radical scavengers on removal of TC,(b) Thermogravimetric analysis (TGA).

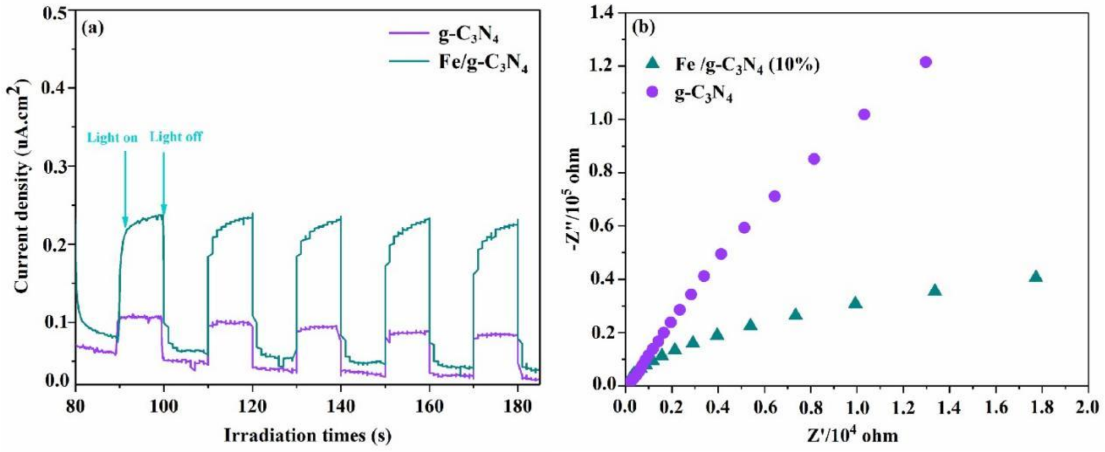

Fig. 15. (a) Photocurrent responses under visible light, (b) EIS Nyquist plots for bulk g-C_3N_4, and Fe/g-C_3N_4 (10%) samples.

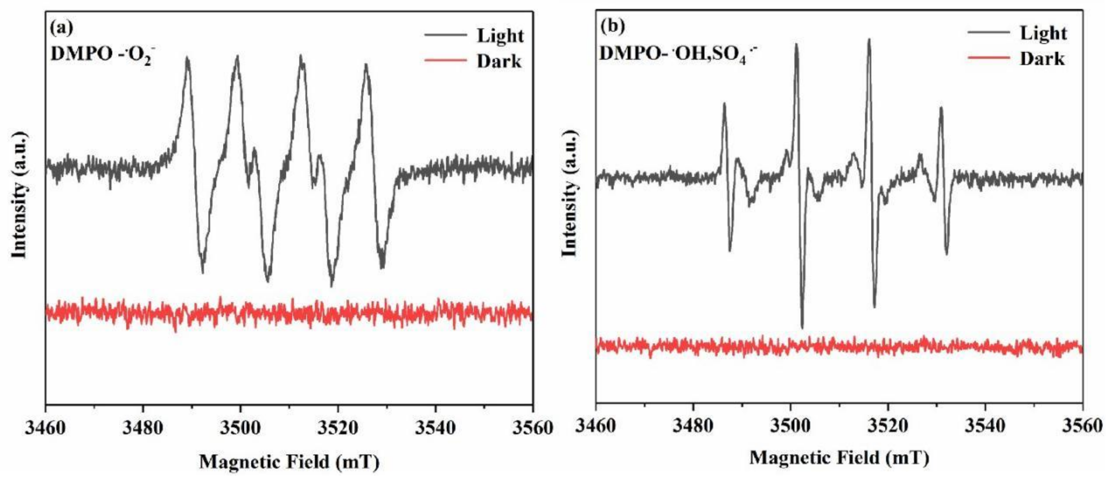

Fig. 16. (a) In methanol dispersion for DMPO−•O_2^- and (b) in aqueous dispersion for DMPO−•OH and $SO_4^{•-}$.

Based on the above results, we proposed the reaction mechanism of Fe/g-C_3N_4 composite material activated PS to remove tetracycline under visible light irradiation (Scheme. 1) and summarized as follows:

$$Fe/g\text{-}C_3N_4 + h\nu \rightarrow e^- + h^+ \tag{1}$$

$$e^- + HSO_5^- \rightarrow SO_4^{\bullet -} + \bullet OH \tag{2}$$

$$Fe^{III} + e^- \rightarrow Fe^{II} \tag{3}$$

$$Fe^{II} + S_2O_8^{2-} + e^- \rightarrow Fe^{III} + SO_4^{\bullet -} + SO_4^{2-} \tag{4}$$

$$SO_4^{\bullet -} + OH^- \rightarrow SO_4^{2-} + \bullet OH \tag{5}$$

$$h^+ + OH^- \rightarrow \bullet OH \tag{6}$$

$$SO_4^{\bullet -} / \bullet OH / h^+ + TC \rightarrow Products \tag{7}$$

Briefly, the conduction band (CB) and valence band (VB) of the Fe/g-C_3N_4 catalyst generated photo-generated electrons (e^-) and photo-generated holes (h^+), respectively (Eq. (1)). There is a synergy between photocatalysis and PS activation process(Eq. (2)). Fe^{3+} and O_2 were reduced by e^- to Fe^{2+} and $\bullet O_2^-$ .The produced ferrous ions, superoxide radicals and holes can effectively activate PS under visible light to produce sulfate radicals ($SO_4^{\bullet -}$) and hydroxyl radicals (•OH) (Eqs. (2)and (3)). The introduction of ferrocene and the conversion between ferrous ions and ferric ions also promoted the activation of persulfate (Eqs. (3) and (4)). Strong oxidizing $SO_4^{\bullet -}$ could effectively remove tetracycline, oxidize and decompose it into carbon dioxide, water and other by-products, and reduce water toxicity(Eqs. (5-7)). Therefore, $SO_4^{\bullet -}$, h^+, and •OH are the main active substances in the Fe/g-C_3N_4 composite material in the visible light activation of PS to remove tetracycline, which can eventually degrade tetracycline into small molecular compounds, and even mineralize it into CO_2, H_2O, etc.

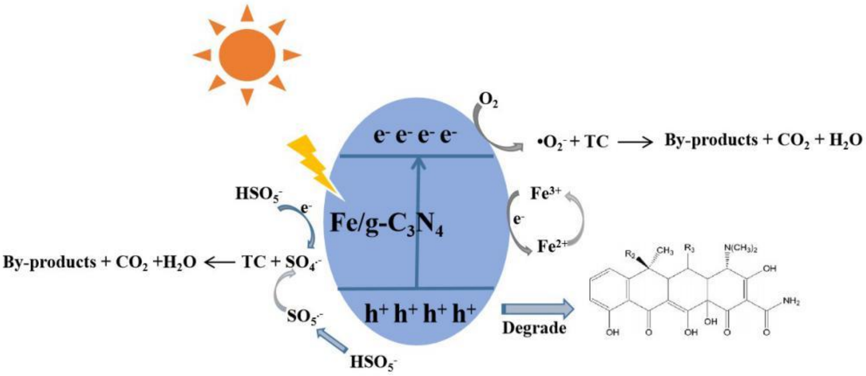

Scheme 1. Degradation mechanisms of TC by Fe-g-C_3N_4 /PMS/Vis process.

4. Conclusions

In summary, Fe/g-C_3N_4 catalysts with various doping ratio were successfully prepared by the calcination method. This study comprehensively explored their catalytic performance toward PS activation under visible light evaluated by TC degradation. Fe/g-C_3N_4 with good photocatalytic performance was synthesized by calcination method, effectively helped the separation of photogenerated carriers, and was beneficial to the activation of PS. When the PS concentration reached 2.5 mM, the Fe/g-C_3N_4/PS/Vis system had a removal rate of 93% for tetracycline after 60 min of visible light reaction. The effects of different ferrocene doping proportions, initial TC concentration, catalyst dosage, PS concentration and pH on the removal of tetracycline by photocatalytic activation of PS were explored. The experimental results showed that when the PS reached 2.5 mM, the catalyst amount was 1 g L^{-1}, and the iron doping amount was 10%, the catalytic activation performance of the composite catalyst was the best. The catalyst had good stability in a wide pH range, where in acidic and neutral conditions were more conducive to the removal of tetracycline.

In the reaction system, the main active species involved in $SO_4^{\bullet-}$, •OH and h^+, of which holes contributed the most. Photocurrent experiments had proved that the modification of ferrocene was beneficial to the separation of photogenerated carriers in g-C_3N_4 and promoted the photocatalytic reaction. As the result of BET, the specific surface area of the composite material was larger, which provided a larger attachment space for the reaction and facilitated the removal of pollutants. Fe/g-C_3N_4 had good stability and recyclability, and its chemical structure was quite stable. It is an effective catalyst for activating PS under visible light to effectively remove tetracycline from water.

Acknowledgements

This work was supported by the National Natural Science Foundation of China (No. 51521006, 51378190, 51039001, 50179011, 51709101, 51879101, 51579098), the National Program for Support of Top–Notch Young Professionals of China (2014), the Program for Changjiang Scholars and Innovative Research Team in University (IRT-13R17), and Hunan Provincial Science and Technology Plan Project (2018SK20410, 2017SK2243, 2016RS3026), and the Fundamental Research Funds for the Central Universities (531119200086, 531118010114, 531107050978, 541109060031).

References

[1] H. Wang, H. Wang, Z. Wang, L. Tang, G. Zeng, P. Xu, M. Chen, T. Xiong, C. Zhou, X. Li, D. Huang, Y. Zhu, Z. Wang, J. Tang, Covalent organic framework photocatalysts: structures and applications, Chem. Soc. Rev. 49 (2020) 4135–4165.

[2] S. Ye, M. Yan, X. Tan, J. Liang, G. Zeng, H. Wu, B. Song, C. Zhou, Y. Yang, H. Wang, Facile assembled biochar-based nanocomposite with improved graphitization for efficient photocatalytic activity driven by visible light, Appl. Catal. B Environ. 250 (2019) 78–88.

[3] X. Wang, Z. Zhou, Z. Liang, Z. Zhuang, Y. Yu, Photochemical synthesis of the Fe^0 /C_3N_4 /MoS_2 heterostructure as a highly active and reusable photocatalyst, Appl. Surf. Sci. 423 (2017) 225–235.

[4] K. Luo, Q. Niu, Y. Zhu, B. Song, G. Zeng, W. Tang, S. Ye, J. Zhang, M. Duan, W. Xing, Desalination behavior and performance of flow-electrode capacitive deionization under various operational modes, Chem. Eng. J. 389 (2020) 124051.

[5] H. Yi, M. Yan, D. Huang, G. Zeng, C. Lai, M. Li, X. Huo, L. Qin, S. Liu, X. Liu, B. Li, H. Wang, M. Shen, Y. Fu, X. Guo, Synergistic effect of artificial enzyme and 2D nano-structured Bi_2WO_6 for eco-friendly and efficient biomimetic photocatalysis, Appl. Catal. B Environ. 250 (2019) 52–62.

[6] W. Wang, Z. Zeng, G. Zeng, C. Zhang, R. Xiao, C. Zhou, W. Xiong, Y. Yang, L. Lei, Y. Liu, D. Huang, M. Cheng, Y. Yang, Y. Fu, H. Luo, Y. Zhou, Sulfur

doped carbon quantum dots loaded hollow tubular g-C_3N_4 as novel photocatalyst for destruction of Escherichia coli and tetracycline degradation under visible light, Chem. Eng. J. 378 (2019) 122132.

[7] Y. Yang, C. Zhang, D. Huang, G. Zeng, J. Huang, C. Lai, C. Zhou, W. Wang, H. Guo, W. Xue, R. Deng, M. Cheng, W. Xiong, Boron nitride quantum dots decorated ultrathin porous g-C_3N_4: Intensified exciton dissociation and charge transfer for promoting visible-light-driven molecular oxygen activation, Appl. Catal. B Environ. 245 (2019) 87–99.

[8] C. Zhou, G. Zeng, D. Huang, Y. Luo, M. Cheng, Y. Liu, W. Xiong, Y. Yang, B. Song, W. Wang, B. Shao, Z. Li, Distorted polymeric carbon nitride via carriers transfer bridges with superior photocatalytic activity for organic pollutants oxidation and hydrogen production under visible light, J. Hazard. Mater. 386 (2020) 121947.

[9] B. Song, J. Gong, W. Tang, G. Zeng, M. Chen, P. Xu, M. Shen, S. Ye, H. Feng, C. Zhou, Y. Yang, Influence of multi-walled carbon nanotubes on the microbial biomass, enzyme activity, and bacterial community structure in 2,4-dichlorophenol-contaminated sediment, Sci. Total Environ. 713 (2020) 136645.

[10] X. Zhou, Z. Zeng, G. Zeng, C. Lai, R. Xiao, S. Liu, D. Huang, L. Qin, X. Liu, B. Li, H. Yi, Y. Fu, L. Li, Z. Wang, Persulfate activation by swine bone char-derived hierarchical porous carbon: Multiple mechanism system for organic pollutant degradation in aqueous media, Chem. Eng. J. 383 (2020)

123091.

[11] W. Li, L. Wang, Q. Zhang, Z. Chen, X. Deng, C. Feng, L. Xu, M. Sun, Fabrication of an ultrathin 2D/2D C_3N_4/MoS_2 heterojunction photocatalyst with enhanced photocatalytic performance, J. Alloys Compd. 808 (2019) 151681.

[12] Y. Yang, G. Zeng, D. Huang, C. Zhang, D. He, C. Zhou, W. Wang, W. Xiong, B. Song, H. Yi, S. Ye, X. Ren, In Situ Grown Single-Atom Cobalt on Polymeric Carbon Nitride with Bidentate Ligand for Efficient Photocatalytic Degradation of Refractory Antibiotics, Small. 16 (2020) 1–12.

[13] Q. Li, N. Zhang, Y. Yang, G. Wang, D.H.L. Ng, High efficiency photocatalysis for pollutant degradation with MoS_2/C_3N_4 heterostructures, Langmuir. 30 (2014) 8965–8972.

[14] J. Kang, Y. Tang, M. Wang, C. Jin, J. Liu, S. Li, Z. Li, J. Zhu, The enhanced peroxymonosulfate-assisted photocatalytic degradation of tetracycline under visible light by g-C3N4/Na-BiVO4heterojunction catalyst and its mechanism, J. Environ. Chem. Eng. 9 (2021) 105524.

[15] J. Li, E. Liu, Y. Ma, X. Hu, J. Wan, L. Sun, J. Fan, Synthesis of MoS 2 /g-C 3 N 4 nanosheets as 2D heterojunction photocatalysts with enhanced visible light activity, Appl. Surf. Sci. 364 (2016) 694–702.

[16] S. Ye, G. Zeng, H. Wu, J. Liang, C. Zhang, J. Dai, W. Xiong, B. Song, S. Wu, J. Yu, The effects of activated biochar addition on remediation efficiency of co-composting with contaminated wetland soil, Resour. Conserv. Recycl. 140 (2019) 278–285.

[17] W. Liu, J. Zhou, Y. Zhou, D. Liu, Peroxymonosulfate-assisted g-C3N4@Bi2MoO6 photocatalytic system for degradation of nimesulide through phenyl ether bond cleavage under visible light irradiation, Sep. Purif. Technol. 264 (2021) 118288.

[18] A.E. Albalawi, A.K. Khalaf, M.S. Alyousif, A.D. Alanazi, P. Baharvand, M. Shakibaie, H. Mahmoudvand, Fe3O4@piroctone olamine magnetic nanoparticles: Synthesize and therapeutic potential in cutaneous leishmaniasis, Biomed. Pharmacother. 139 (2021) 111566.

[19] M.A. Alcudia-Ramos, M.O. Fuentez-Torres, F. Ortiz-Chi, C.G. Espinosa-González, N. Hernández‐Como, D.S. García-Zaleta, M.K. Kesarla, J.G. Torres-Torres, V. Collins-Martínez, S. Godavarthi, Fabrication of g-C_3N_4/TiO_2 heterojunction composite for enhanced photocatalytic hydrogen production, Ceram. Int. 46 (2020) 38–45.

[20] L. Zeng, S. Li, X. Li, J. Li, S. Fan, X. Chen, Z. Yin, M. Tadé, S. Liu, Visible-light-driven sonophotocatalysis and peroxymonosulfate activation over 3D urchin-like MoS_2/C nanoparticles for accelerating levofloxacin elimination: Optimization and kinetic study, Chem. Eng. J. 378 (2019) 122039.

[21] S.L. Prabavathi, K. Govindan, K. Saravanakumar, A. Jang, V. Muthuraj, Construction of heterostructure CoWO4/g-C3N4 nanocomposite as an efficient visible-light photocatalyst for norfloxacin degradation, J. Ind. Eng. Chem. 80 (2019) 558–567.

[22] W. Tao, M. Wang, R. Ali, S. Nie, Q. Zeng, R. Yang, W.M. Lau, L. He, H.

Tang, X. Jian, Multi-layered porous hierarchical TiO_2/g-C_3N_4 hybrid coating for enhanced visible light photocatalysis, Appl. Surf. Sci. 495 (2019) 143435.

[23] C. Hu, E. Lei, K. Hu, L. Lai, D. Zhao, W. Zhao, H. Rong, Simple synthesis of 3D flower-like g-C_3N_4/TiO_2 composite microspheres for enhanced visible-light photocatalytic activity, J. Mater. Sci. 55 (2020) 151–162.

[24] R. Guan, J. Li, J. Zhang, Z. Zhao, D. Wang, H. Zhai, D. Sun, Photocatalytic Performance and Mechanistic Research of ZnO/g-C_3N_4 on Degradation of Methyl Orange, ACS Omega. 4 (2019) 20742–20747.

[25] B. Gao, J. Wang, M. Dou, C. Xu, X. Huang, Enhanced photocatalytic removal of amoxicillin with Ag/TiO_2/mesoporous g-C3N4 under visible light: property and mechanistic studies, Environ. Sci. Pollut. Res. 27 (2020) 7025–7039.

[26] V. Hasija, V.H. Nguyen, A. Kumar, P. Raizada, V. Krishnan, A.A.P. Khan, P. Singh, E. Lichtfouse, C. Wang, P. Thi Huong, Advanced activation of persulfate by polymeric g-C3N4 based photocatalysts for environmental remediation: A review, J. Hazard. Mater. 413 (2021) 125324.

[27]M. Sabri, A. Habibi-Yangjeh, H. Chand, V. Krishnan, Activation of persulfate by novel TiO2/FeOCl photocatalyst under visible light: Facile synthesis and high photocatalytic performance, Sep. Purif. Technol. 250 (2020) 117268.

[28]S. Asadzadeh-Khaneghah, A. Habibi-Yangjeh, D. Seifzadeh, H. Chand, V. Krishnan, G-C3N4 nanosheets adhered with Ag3BiO3 and carbon dots with appreciably promoted photoactivity towards elimination of several contaminants, Adv. Powder Technol. 32 (2021) 1196–1206.

[29]H. Wang, X. Yuan, Y. Wu, G. Zeng, W. Tu, C. Sheng, Y. Deng, F. Chen, J.W. Chew, Plasmonic Bi nanoparticles and BiOCl sheets as cocatalyst deposited on perovskite-type ZnSn(OH)6 microparticle with facet-oriented polyhedron for improved visible-light-driven photocatalysis, Appl. Catal. B Environ. 209 (2017) 543–553.

[30] S. Liu, S. Wang, Y. Jiang, Z. Zhao, G. Jiang, Z. Sun, Synthesis of Fe_2O_3 loaded porous g-C3N4 photocatalyst for photocatalytic reduction of dinitrogen to ammonia, Chem. Eng. J. 373 (2019) 572–579.

[31] S. Ghafoor, A. Inayat, F. Aftab, H. Duran, K. Kirchhoff, S. Waseem, S.N. Arshad, TiO_2 nanofibers embedded with g-C3N4 nanosheets and decorated with Ag nanoparticles as Z-scheme photocatalysts for environmental remediation, J. Environ. Chem. Eng. 7 (2019) 1–10.

[32] C. Guan, J. Jiang, S. Pang, J. Ma, X. Chen, T.T. Lim, Nonradical transformation of sulfamethoxazole by carbon nanotube activated peroxydisulfate: Kinetics, mechanism and product toxicity, Chem. Eng. J. 378 (2019) 122147.

[33] H. Li, C. Shan, B. Pan, Development of Fe-doped g-C_3N_4/graphite mediated peroxymonosulfate activation for degradation of aromatic pollutants via nonradical pathway, Sci. Total Environ. 675 (2019) 62–72.

[34] S. Wu, Y. Lin, C. Yang, C. Du, Q. Teng, Y. Ma, D. Zhang, L. Nie, Y. Zhong, Enhanced activation of peroxymonosulfte by $LaFeO_3$ perovskite supported on Al2O3 for degradation of organic pollutants, Chemosphere. 237 (2019)

124478.

[35] S. Wu, H. Li, X. Li, H. He, C. Yang, Performances and mechanisms of efficient degradation of atrazine using peroxymonosulfate and ferrate as oxidants, Chem. Eng. J. 353 (2018) 533–541.

[36] K.Y.A. Lin, J.T. Lin, Ferrocene-functionalized graphitic carbon nitride as an enhanced heterogeneous catalyst of Fenton reaction for degradation of Rhodamine B under visible light irradiation, Chemosphere. 182 (2017) 54–64.

[37] Y. Yang, C. Zhou, W. Wang, W. Xiong, G. Zeng, D. Huang, C. Zhang, B. Song, W. Xue, X. Li, Z. Wang, D. He, H. Luo, Z. Ouyang, Recent advances in application of transition metal phosphides for photocatalytic hydrogen production, Chem. Eng. J. 405 (2021) 126547.

[38] J. Zhou, W. Liu, W. Cai, The synergistic effect of Ag/AgCl@ZIF-8 modified g-C3N4 composite and peroxymonosulfate for the enhanced visible-light photocatalytic degradation of levofloxacin, Sci. Total Environ. 696 (2019) 133962.

[39] Z. Hu, J. Lyu, M. Ge, Role of reactive oxygen species in the photocatalytic degradation of methyl orange and tetracycline by Ag_3PO4 polyhedron modified with g-C_3N_4, Mater. Sci. Semicond. Process. 105 (2020) 104731.

[40] W. Da Oh, C.Z. Ng, S.L. Ng, J.W. Lim, K.H. Leong, Rapid degradation of organics by peroxymonosulfate activated with ferric ions embedded in graphitic carbon nitride, Sep. Purif. Technol. 230 (2020) 115852.

[41] J. Fan, H. Qin, S. Jiang, Mn-doped g-C_3N_4 composite to activate

peroxymonosulfate for acetaminophen degradation: The role of superoxide anion and singlet oxygen, Chem. Eng. J. 359 (2019) 723–732.

[42] L. Dong, T. Xu, W. Chen, W. Lu, Synergistic multiple active species for the photocatalytic degradation of contaminants by imidazole-modified g-C_3N_4 coordination with iron phthalocyanine in the presence of peroxymonosulfate, Chem. Eng. J. 357 (2019) 198–208.

[43] H. Li, C. Shan, B. Pan, Fe(III)-Doped g-C3N4 Mediated Peroxymonosulfate Activation for Selective Degradation of Phenolic Compounds via High-Valent Iron-Oxo Species, Environ. Sci. Technol. 52 (2018) 2197–2205.

[44] J. Li, Y. Wan, Y. Li, G. Yao, B. Lai, Surface Fe(III)/Fe(II) cycle promoted the degradation of atrazine by peroxymonosulfate activation in the presence of hydroxylamine, Appl. Catal. B Environ. 256 (2019) 117782.

[45] L. Wang, X. Guo, Y. Chen, S. Ai, H. Ding, Cobalt-doped g-C_3N_4 as a heterogeneous catalyst for photo-assisted activation of peroxymonosulfate for the degradation of organic contaminants, Appl. Surf. Sci. 467–468 (2019) 954–962.

[46] C. Liu, L. Liu, X. Tian, Y. Wang, R. Li, Y. Zhang, Z. Song, B. Xu, W. Chu, F. Qi, A. Ikhlaq, Coupling metal–organic frameworks and g-C_3N_4 to derive Fe@N-doped graphene-like carbon for peroxymonosulfate activation: Upgrading framework stability and performance, Appl. Catal. B Environ. 255 (2019) 117763.

[47] Y. Liu, W. Guo, H. Guo, X. Ren, Q. Xu, Cu (II)-doped V_2O_5 mediated

persulfate activation for heterogeneous catalytic degradation of benzotriazole in aqueous solution, Sep. Purif. Technol. 230 (2020) 115848.

[48] M. Wei, X. Shi, L. Xiao, H. Zhang, Synthesis of polyimide-modified carbon nanotubes as catalyst for organic pollutant degradation via production of singlet oxygen with peroxymonosulfate without light irradiation, J. Hazard. Mater. 382 (2020) 120993.

[49] J.M. Dangwang Dikdim, Y. Gong, G.B. Noumi, J.M. Sieliechi, X. Zhao, N. Ma, M. Yang, J.B. Tchatchueng, Peroxymonosulfate improved photocatalytic degradation of atrazine by activated carbon/graphitic carbon nitride composite under visible light irradiation, Chemosphere. 217 (2019) 833–842.

[50] H. Sun, C.K. Kwan, A. Suvorova, H.M. Ang, M.O. Tadé, S. Wang, Catalytic oxidation of organic pollutants on pristine and surface nitrogen-modified carbon nanotubes with sulfate radicals, Appl. Catal. B Environ. 154–155 (2014) 134–141.

[51] Y. Shang, C. Chen, P. Zhang, Q. Yue, Y. Li, B. Gao, X. Xu, Removal of sulfamethoxazole from water via activation of persulfate by Fe_3C@NCNTs including mechanism of radical and nonradical process, Chem. Eng. J. 375 (2019) 122004.

[52] J. Guo, Y. Zhou, Transformation of heavy metals and dewaterability of waste activated sludge during the conditioning by Fe^{2+}-activated peroxymonosulfate oxidation combined with rice straw biochar as skeleton builder, Chemosphere. 238 (2020) 124628.

[53] Y. Shi, C. Liu, L. Fu, F. Yang, Y. Lv, B. Yu, Hierarchical assembly of polystyrene/graphitic carbon nitride/reduced graphene oxide nanocomposites toward high fire safety, Compos. Part B Eng. 179 (2019) 107541.

[54] P. Lin, J. Shen, X. Yu, Q. Liu, D. Li, H. Tang, Construction of Ti_3C_2 MXene/O-doped g-C_3N_4 2D-2D Schottky-junction for enhanced photocatalytic hydrogen evolution, Ceram. Int. 45 (2019) 24656–24663.

[55] Y. Leng, W. Guo, X. Shi, Y. Li, A. Wang, F. Hao, L. Xing, Degradation of Rhodamine B by persulfate activated with Fe3O4: Effect of polyhydroquinone serving as an electron shuttle, Chem. Eng. J. 240 (2014) 338–343.

[56] X. Song, C. Ren, Q. Zhao, B. Su, Simultaneous removal of Cr(VI) and triclosan from aqueous solutions through Fe_3O_4 magnetic nanoscale-activated persulfate oxidation, Chem. Eng. J. 381 (2020) 122586.

[57] Z. Dong, Q. Zhang, B.Y. Chen, J. Hong, Oxidation of bisphenol A by persulfate via Fe_3O_4-A-MnO_2 nanoflower-like catalyst: Mechanism and efficiency, Chem. Eng. J. 357 (2019) 337–347.

[58] C. Tan, X. Lu, X. Cui, X. Jian, Z. Hu, Y. Dong, X. Liu, J. Huang, L. Deng, Novel activation of peroxymonosulfate by an easily recyclable VC@Fe_3O_4 nanoparticles for enhanced degradation of sulfadiazine, Chem. Eng. J. 363 (2019) 318–328.

[59] Q. Zhang, J. Wang, X. Ye, Z. Hui, L. Ye, X. Wang, S. Chen, Self-Assembly of CdS/$CdIn_2S_4$ Heterostructure with enhanced photocascade synthesis of schiff base compounds in an aromatic alcohols and nitrobenzene system with visible

Light, ACS Appl. Mater. Interfaces. 11 (2019) 46735–46745.

[60] J. Li, Q. Liu, Q. qing Ji, B. Lai, Degradation of p-nitrophenol (PNP) in aqueous solution by Fe^0-PM-PS system through response surface methodology (RSM), Appl. Catal. B Environ. 200 (2017) 633–646.

[61] Y. Wang, H. Sun, X. Duan, H.M. Ang, M.O. Tadé, S. Wang, A new magnetic nano zero-valent iron encapsulated in carbon spheres for oxidative degradation of phenol, Appl. Catal. B Environ. 172–173 (2015) 73–81.

[62] H. Sun, G. Zhou, S. Liu, H.M. Ang, M.O. Tadé, S. Wang, Nano-Fe^0 encapsulated in microcarbon spheres: Synthesis, characterization, and environmental applications, ACS Appl. Mater. Interfaces. 4 (2012) 6235–6241.

[63] J. Zhou, W. Liu, W. Cai, The synergistic effect of Ag/AgCl@ZIF-8 modified g-C_3N_4 composite and peroxymonosulfate for the enhanced visible-light photocatalytic degradation of levofloxacin, Sci. Total Environ. 696 (2019) 133962.

[64] H. Zheng, J. Bao, Y. Huang, L. Xiang, Faheem, B. Ren, J. Du, M.N. Nadagouda, D.D. Dionysiou, Efficient degradation of atrazine with porous sulfurized Fe_2O_3 as catalyst for peroxymonosulfate activation, Appl. Catal. B Environ. 259 (2019) 118056.

[65] M. Dong, J. Yu, J. Wang, Q. Zhang, W. Lin, Construction of phenyl-grafted carbon nitride for enhancing the visible-light activity, Chem. Phys. Lett. 737 (2019) 136817.

[66] Y. Zhou, Y. Gao, J. Jiang, Y.M. Shen, S.Y. Pang, Z. Wang, J. Duan, Q. Guo, C.

Guan, J. Ma, Transformation of tetracycline antibiotics during water treatment with unactivated peroxymonosulfate, Chem. Eng. J. 379 (2020) 122378.

[67] S. Zhang, H. Gao, X. Xu, R. Cao, H. Yang, X. Xu, J. Li, MOF-derived CoN/N-C@SiO_2 yolk-shell nanoreactor with dual active sites for highly efficient catalytic advanced oxidation processes, Chem. Eng. J. 381 (2020) 122670.

[68] S. Li, Y. Tang, M. Wang, J. Kang, C. Jin, J. Liu, Z. Li, J. Zhu, NiO/g-C3N4 2D/2D heterojunction catalyst as efficient peroxymonosulfate activators toward tetracycline degradation: characterization, performance and mechanism, J. Alloys Compd. 880 (2021) 160547.